

Observatório Nacional
Ministério da Ciência, Tecnologia e Inovação
Programa de Pós-Graduação em Geofísica

Dissertação de mestrado

HOW DO EXTERNAL MAGNETIC FIELDS INFLUENCE GEOMAGNETIC JERK
DETECTION?

Diego Andrés Peñá Arcos

Orientadora:

Katia Jasbinschek dos Reis Pinheiro

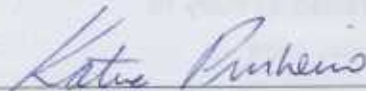
Rio de Janeiro 2012

"EXTERNAL MAGNETIC FIELDS INFLUENCE GEOMAGNETIC JERK
DETECTION?"

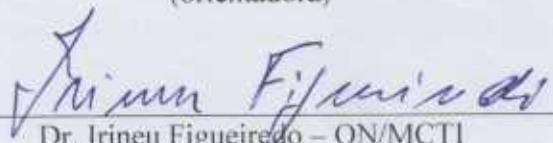
DIEGO ANDRÉS PEÑA ARCOS

DISSERTAÇÃO SUBMETIDA AO CORPO DOCENTE DO PROGRAMA DE PÓS-GRADUAÇÃO EM GEOFÍSICA DO OBSERVATÓRIO NACIONAL COMO PARTE DOS REQUISITOS NECESSÁRIOS PARA A OBTENÇÃO DO GRAU DE MESTRE EM GEOFÍSICA.

Aprovada por:



Dra. Kátia Jasbinschek dos Reis Pinheiro – ON/MCTI
(orientadora)



Dr. Irineu Figueiredo – ON/MCTI



Dr. Odim Mendes Junior – INPE

RIO DE JANEIRO – BRASIL

28 DE FEVEREIRO DE 2013

*Si quieres cambio verdadero,
pues camina distinto.*

C13

Resumo

Os impulsos da variação secular geomagnética são importantes para compreender melhor a dinâmica do núcleo terrestre e a condutividade elétrica do manto. Embora a origem dos impulsos seja interna, sua detecção em dados de observatório e de satélite é muito influenciada pelas contribuições do campo magnético externo. No presente trabalho foi quantificada a influencia do campo magnético externo na detecção dos impulsos geomagnéticos. Foram comparadas as detecções dos impulsos de 1969, 1978 e 1991 (nos componentes X, Y e Z) em dois conjuntos de dados obtidos do modelo de campo magnético CM4: o primeiro conjunto só considera o campo magnético do núcleo e o segundo, além do campo do núcleo, considera os campos externo e induzido da magnetosfera e a ionosfera, calculados em 186 observatórios magnéticos. Os resultados desta pesquisa mostram como os campos externo e induzido influenciam as diferentes componentes do campo magnético e as feições da detecção dos impulsos, como as barras de erro e atrasos diferenciais.

How do external magnetic fields influence geomagnetic jerk detection?

Diego Peña, Katia Pinheiro

Abstract

Jerks are important for a better understanding of core dynamics and mantle electrical conductivity. Although jerks have an internal origin, their detection in observatory and satellite data are highly influenced by the external magnetic field contributions. We compared the detection of the 1969, 1978 and 1991 jerks (X, Y and Z components) in two datasets derived from CM4 field model: the first considering only the Core magnetic field and the second beyond the core field considering the external and induced fields of Magnetosphere and Ionosphere calculated in 186 magnetic observatories. The results of this investigation quantified how external and induced fields influenced on different components of the magnetic field and on jerk detections characteristics such error bars and differential time delays.

1 Introduction

The temporal variations of the geomagnetic field are caused by different sources: an internal field generated by the fluid flow in the outer core, induced fields in the crust and mantle, and external fields caused by the solar wind interaction with the core magnetic field. These variations include a wide time-scale, from seconds to hours (external origin), from months to decades (overlapping between external and internal sources) and millennial periods (internal origin).

The geomagnetic secular variation (SV) is defined as the first time derivative of the magnetic field, using annual or monthly means data from magnetic observatories and satellites. The SV is divided by intervals of approximately linear trends separated by abrupt changes on its slopes. These rapid changes of the SV take place in a short time of about two years and are called geomagnetic jerks (Mandea *et al.*, 2010).

Courtillot *et al.* (1978) was the first to observe geomagnetic jerks, through the analysis of observatory annual means datasets. They detected an impulse in 1970 in the Y component at European observatories. Many geomagnetic jerks have occurred in the past and show different characteristics: 1901, 1913, 1925 being possibly global in extent, the 1932 and 1949 jerks observed only in the Pacific and American areas and the 1969, 1978 and 1991 jerks were found worldwide (Alexandrescu *et al.*, 1996; Le Huy *et al.*, 1998; Pinheiro *et al.*, 2011). More recent jerks were also detected in 1999 (De Michelis & Tozzi, 2005; Mandea *et al.*, 2000), 2003 (Olsen & Mandea, 2007), 2005 (Olsen & Mandea, 2008) and 2007 (Chulliat *et al.*, 2010).

Jerks may be detected and characterized by different methods, such as fitting of straight lines, wavelet analysis and identification of jerks in global field models (Alexandrescu *et al.*, 1995; Le Huy *et al.*, 1998; Sabaka *et al.*, 2004).

The internal origin of jerks was demonstrated by Malin & Hodder (1982) using spherical harmonic analysis. They showed that internal sources may give rise to changes in secular variation on time-scales as short as one or two years. On the other hand, Alldredge (1977, 1984) suggested that some external signal may contribute to intensify the observed jerk. Jerks are usually detected in the secular variation of the Y magnetic field component since it is less influenced by external signals.

Besides the internal origin of jerks is well established, it is important to analyze the possible influence of external fields as artefacts on the jerks detection. Verbanac *et al.* (2006) showed that the X component in observatory annual means was influenced by external fields, mainly by the ring current.

In this work we analyzed the 1969, 1978 and 1991 jerk detections considering the North (X), East (Y) and vertical (Z) components. We used the CM4 comprehensive model (Sabaka *et al.*, 2004) to calculate two datasets and quantify how much external and induced fields may influence on jerks occurrence times and its error bars. Section 2 presents in detail the model dataset used; section 3 presents how external fields may affect on main field signal; section 4 describes the methodology used to detect jerks and to quantify the influence of external and induced fields; section 5 presents the results and leded some discussions about them; and section 6 presents the main conclusions obtained from this work, respectively.

2 Model Dataset

Hourly model data from 1960 to 2000 for X, Y and Z field components were calculated using the CM4 field model (Sabaka *et al.*, 2002; 2004) in the same locations of the 186 magnetic observatories chosen by Pinheiro *et al.*, (2011). We calculated two datasets, as exemplified in Figure 1: only Core magnetic field data (here identified as CORE) and Core field added with External and Induced fields (here identified as COEI).

The comprehensive model (CM4) of the Earth's magnetic field was derived from observatory data (from 1960 to 2000) as well as data from POGO (1965-1971), Magsat (November, 1979 - May, 1980), Ørsted (from February, 1999) and CHAMP (from July, 2000) satellite missions.

The advantage of CM4 model is its ability to separate the different sources of the magnetic field (Sabaka *et al.*, 2004). For core field data, a spherical harmonic expansion up to degree 15 was used. The external and induced fields data use the primary and induced fields of ionosphere and magnetosphere generated by the same field model. The primary ionospheric field is represented as currents which flowing in a thin spherical shell at 110 km of altitude. The ionospheric parametrization employs harmonic functions with symmetry supplied by a quasi-dipole coordinate system, which is aligned with the ambient magnetic field and offers a high latitudinal resolution in order to fit the equatorial electrojet (EEJ). Induced contributions are modeled by using a four layer, 1D, radially electrical conductivity model of the mantle derived from Sq and Dst data at selected European observatories (Olsen, 1998).

The main sources of the primary magnetospheric field are currents that flowing in the magnetotail, magnetopause and ring current complexes. Near the Earth, the field is calculated as the negative gradient of a potential function represented by an external spherical harmonic expansion in dipole coordinates, which has regular daily and seasonal periodicities. The ring current variability is modeled as a linear function of the Dst index for external dipole terms only (see Sabaka *et al.*, 2002).

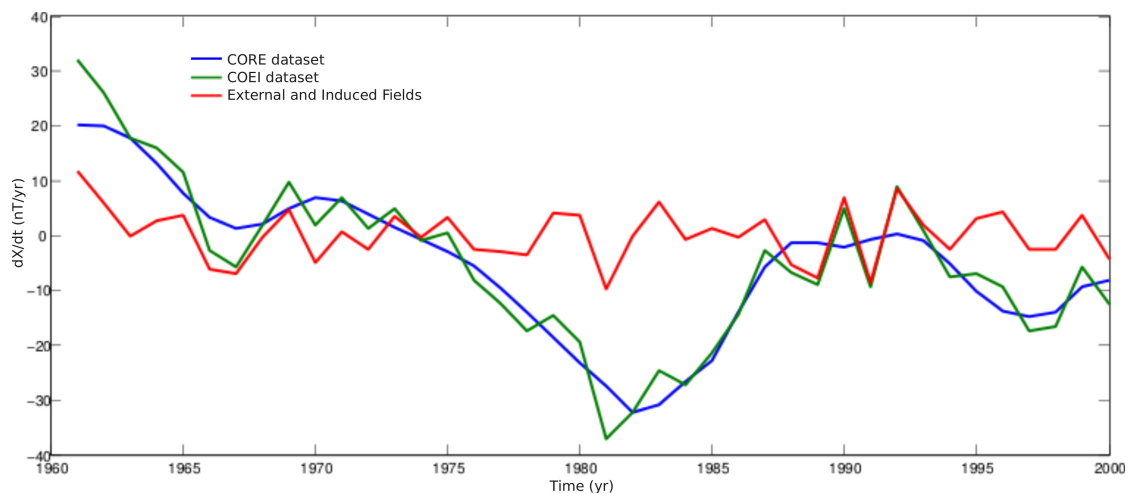


Figure 1: Secular variation calculated from annual means of X field component in Alma Ata observatory location (AAA, Kazakhstan) for core field (CORE, blue line), core and external fields (COEI, green line) and external field (Magnetosphere and Ionosphere, red line).

The induced contributions of the magnetosphere are treated in a similar manner as the ionosphere and are thus coupled with an internal spherical harmonic expansion using the same conductivity model. The influence of solar activity is represented by an amplification factor assumed to be equal for all harmonics.

3 External Field Influences

The variability of external magnetic fields is mainly associated to the interaction between the solar wind and Earth's core magnetic field. In observatory and satellite data, the separation between internal and external fields is not straightforward. The analysis of the external field hourly means in the CM4 model data reveals daily, monthly, seasonal, annual and 11/22 - years variations. In order to reduce the influence of external fields in main field data, we calculated annual means of magnetospheric and ionospheric fields and compared with the internal field variation (Figure 1). Annual means reduces strongly the daily, monthly and seasonal variations, but long-term variations still persists.

The amplitude of external and induced fields variation in CM4 is significant if compared with the main field signal, as shown in Figure 1. These variations cause substantial disturbance that may change jerk detection characteristics, such as occurrence time, amplitude and their error bars. The rapid changes in the external field signals modify the smoothness of the main field signal, accentuating or minimizing the jerk detection. This disturbance is increased in the neighborhood of the occurrence times by their coincidence with the maximum solar activities.

In the studied period (1960-2000), three complete solar cycles were registered (cycles 20, 21 and 22; see Figure 2). Magnetic storms are known to be more frequent approximately during solar maximums (Le *et al.*, 2012) and thus may cause alteration even in the annual means dataset. The comparison of the solar cycle with the annual variation of the external field showed a good correlation between the zones with low solar activity and the zones with small external field variability (Figure 2).

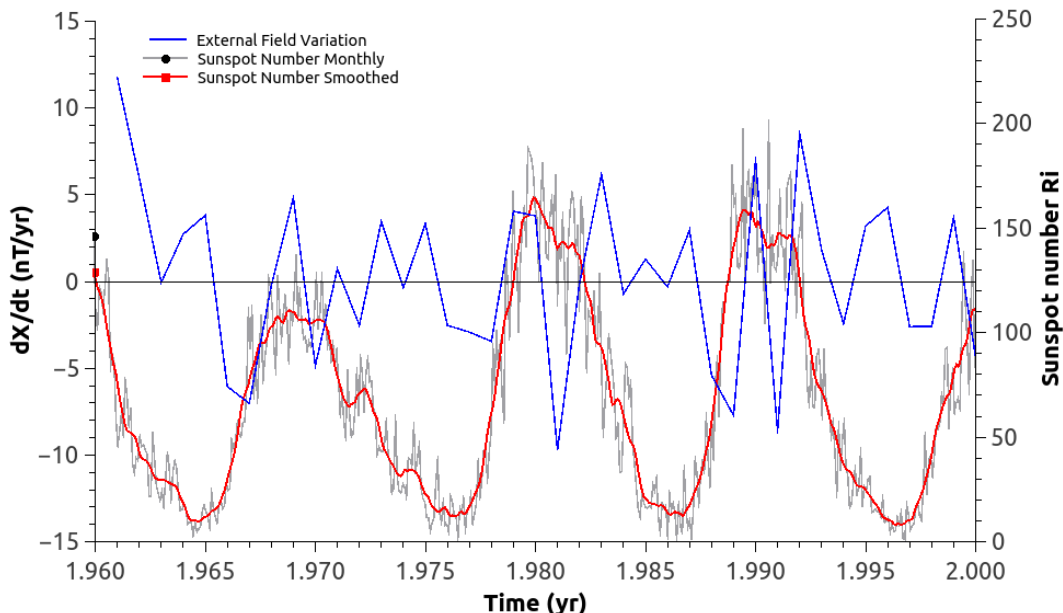


Figure 2: Comparison between the external fields variation and the solar cycle. Blue line represents the annual means variation of X component of external fields (magnetosphere and ionosphere, primary and induced fields) in Alma Alta observatory (AAA, Kazakhstan). Red and gray lines represent the sunspot number smoothed and monthly means, respectively. Smooth values are an average of 13 monthly observed values centered on the month of concern (NOAA/SWPC Boulder, CO USA).

The annual means of external and induced fields, presented similar variation trends but different amplitudes in different geographical locations. The amplitudes depend on the CM4 parametrization for external fields in different latitudes. For example, observatories near the equatorial electrojet presented larger amplitudes than others located in higher latitudes. It demonstrates that regional representation of external fields by the CM4 model is well comparable with direct observations.

4 Methodology

4.1 Jerk Detection

In order to analyze each jerk separately, the SV series was divided in time windows of 15 years: 7 years before and 7 years after the supposed jerk occurrence time (1969, 1978 and 1991). The identification of jerks occurrence time in this work followed the methodology suggested by Pinheiro *et al.*, (2011). Geomagnetic jerks were modeled as two straight-line segments fitted to secular variation estimates of a geomagnetic element $\dot{C}(t)$ using least-squares (L2) measurement of misfit:

$$\dot{C} = a_1(t - t_0) + b \quad \text{for } t \leq t_0 \quad (1)$$

and

$$\dot{C} = a_2(t - t_0) + b \quad \text{for } t \geq t_0 \quad (2)$$

where t_0 is the occurrence time, a_1 , a_2 , and b are model parameters (Figure 3A) and the jerk amplitude A is given by:

$$A = a_2 - a_1 \quad (3)$$

The preferred model for each jerk is chosen according to the minimum of the misfit curve (Figure 3B) and the error bars determined by a standard deviation σ (a interval with 67% of confidence) on the associated probability distribution function (PDF) curve (Figure 3C).

Jerks are classified as *not detected* when the minimum of the misfit curve (or maximum in the PDF curve) is in one of the extremes of the time window. Jerks are classified as *excluded* when it is not possible to obtain error bars because the area under the PDF curve is less than 67%. Jerks are also classified as *excluded* when the error bars of t_0 and A are greater than 3 yr and 3 nT/yr^2 , respectively.

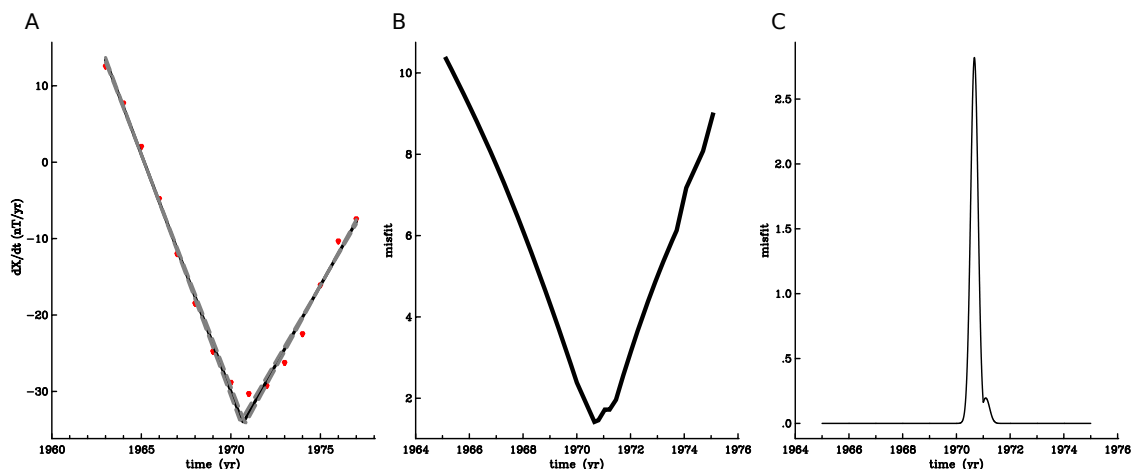


Figure 3: (A) 1969 geomagnetic jerk detected at the X component in Trivandrum observatory location (TRD, India) in CORE dataset and its associated (B) Misfit curve and (C) PDF curve.

4.2 External Field Evaluation

External field influence in jerk detection was quantified by detecting each jerk in each location in CORE dataset (only core field data) and in COEI dataset (core field added external and induced fields data). We compared the results where jerks had been detected in both model data. In this work, we analyzed the occurrence time and amplitude considering their error bars.

We calculated the occurrence time difference Δt_0 for each location corresponding to each magnetic observatory by:

$$\Delta t_{0j} = t_{Ej} - t_{Ij} \quad (4)$$

where t_E and t_I are the jerk occurrence times detected in COEI and CORE datasets, respectively ("E" stands for external and "I" for internal). In the case of a *negative occurrence time difference* ($t_E < t_I$), external fields influence jerks to be detected *apparently earlier* (example in Figure 4A and 4B). In *positive occurrence time differences* ($t_E > t_I$), external fields cause a *apparent delay* in the jerk detection (example in Figure 4C and 4D).

As well as, the differences present positive and negative differences, we used their absolute values to calculate a global quantification of the external influences in jerk detection, the *mean absolute occurrence time difference* $|\Delta t_0|$, that it is given by:

$$|\Delta t_0| = \sum_j \frac{|t_{Ej} - t_{Ij}|}{N} \quad (5)$$

where N is the number of locations where the jerk was detected in both datasets.

The error bar differences (Δe_{min} for the minimum and Δe_{max} for the maximum) were calculated by:

$$\Delta e_j = e_{Ej} - e_{Ij} \quad (6)$$

where e_E and e_I are the error bars (minimum and maximum) detected in COEI and CORE datasets, respectively. They were also calculated in order to quantify whether the external fields disturbed the data.

5 Results and Discussion

In order to characterize and quantify external field influences on the detection of 1969, 1978 and 1991 jerks, we compared in CORE and COEI datasets: the number of locations where jerks were detected, not detected and excluded, the mean occurrence times, the difference between the occurrence time for each location and the mean error bars difference.

The results were presented by each component (X, Y and Z) and they are summarized below. Each geomagnetic jerk was detected in CORE dataset and COEI dataset in time windows of 15 years centered on 1969, 1978 and 1991 for 186 locations correspondent to magnetic observatories studied by Pinheiro *et al.*, 2011.

5.1 X Field Component

5.1.1 1969 Geomagnetic Jerk (X component)

As expected, the 1969 jerk was best detected in CORE model data: it was identified in 86% of the 186 chosen locations and only in 62.4% in the COEI dataset (Table 1). The effect of external fields also caused an increase in the number of excluded model data in COEI. The 1969 jerk (X component) was only detected in 116 locations in both CORE and COEI datasets.

Considering the mean error bars, the mean occurrence time \bar{t}_0 in the two model datasets are similar, but considerably different from the real data results (1969.26). The occurrence time differences (Δt_0) are similar for CORE and COEI because of similar number of locations with positive occurrence time differences ($\Delta t_0 > 0$) and locations with negative occurrence time differences ($\Delta t_0 < 0$). This result shows that, in general, jerks were not preferentially anticipated or delayed in COEI dataset for the 1969 jerk (X component). However, the calculation of $|\Delta t_0| = 1.27$ years revealed high differences in individual locations. For example, Port-aux-Francais observatory location (PAF, French Southern and Antarctic Lands) exhibit a occurrence time difference of 5.64 years due to the external fields influence. In addition, an interesting feature was observed in the results: from 58 locations where the 1969 jerk was detected before in the COEI, 55 of these presented jerks with positive amplitude, as shown in Figure 4A and 4B. On the other hand, from 55 locations where the jerk was detected before in the CORE, 54 of them presented negative amplitudes, as exemplified in Figure 4C and 4D.

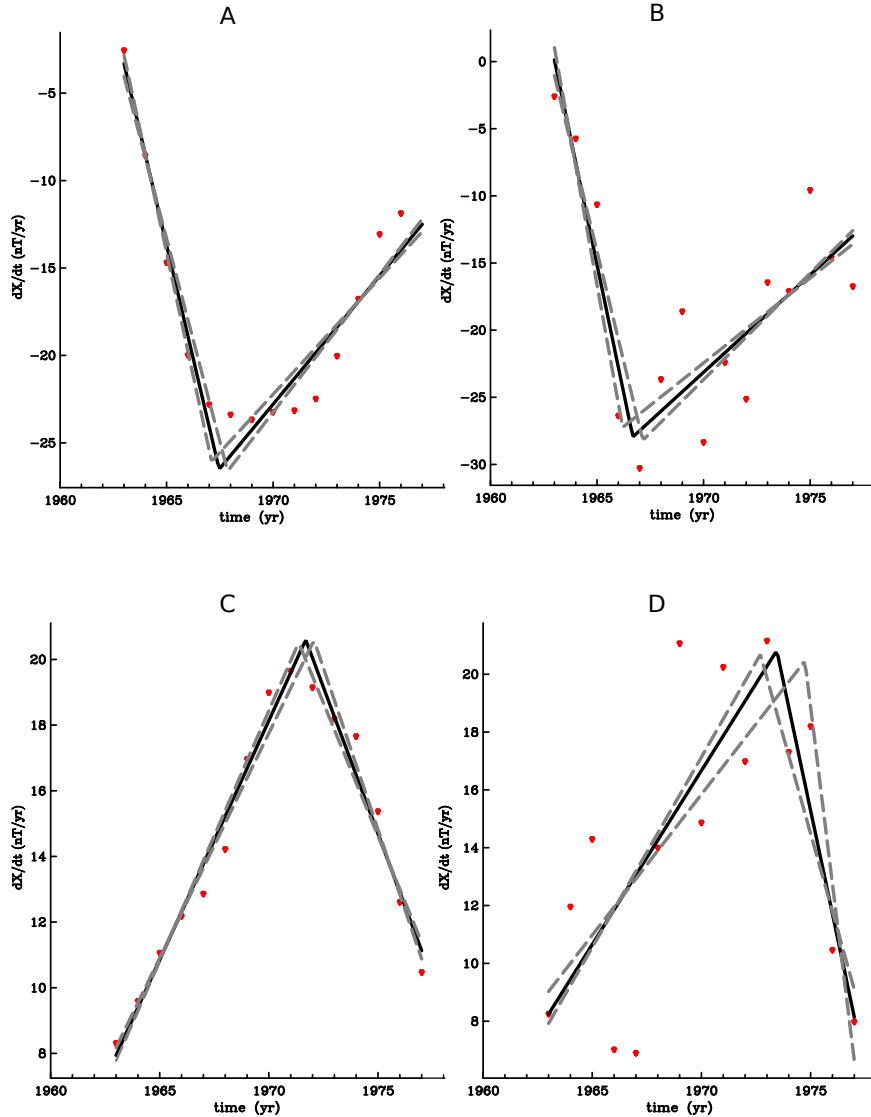


Figure 4: Detection of 1969 jerk in the X component in Beijing Observatory (BJI, China) location in (A) CORE and (B) COEI datasets. Solid line shows the best fit and shaped lines show the error bars. The detected jerk showed positive amplitude and a V-shaped form. The detection date for (A) CORE was 1967.47 and for (B) COEI was 1966.68. Detection of 1969 jerk in the X component in Grocka Observatory (GCK, Serbia) location in (C) CORE and (D) COEI data sets. The detected jerk showed negative amplitude and an inverted V-shaped form. The detection date for (A) CORE was 1971.69 and for (B) COEI was 1973.45. The external influences produce a clear difference in the occurrence time between CORE and COEI datasets.

Table 1: Jerk detection for CORE and COEI model datasets in the X component of the 1969, 1978 and 1991 jerks. DET, EXC and NOT, are the locations where this jerk was detected, excluded and not detected, respectively. The mean occurrence time is \bar{t}_0 . The mean error bars are \bar{e}_{min} and \bar{e}_{max} .

| Jerk | Dataset | DET | EXC | NOT | \bar{t}_0 | \bar{e}_{min} | \bar{e}_{max} |
|------|---------|-----|-----|-----|-------------|-----------------|-----------------|
| 1969 | CORE | 160 | 17 | 9 | 1970.53 | -0.55 | 0.58 |
| | COEI | 116 | 57 | 13 | 1970.22 | -0.74 | 0.84 |
| 1978 | CORE | 134 | 31 | 21 | 1976.59 | -0.69 | 0.73 |
| | COEI | 93 | 81 | 12 | 1977.63 | -1.05 | 1.07 |
| 1991 | CORE | 149 | 30 | 7 | 1992.12 | -0.75 | 0.68 |
| | COEI | 67 | 109 | 10 | 1991.59 | -1.29 | 1.29 |

The global distribution of the differences of X component (Figure 5) showing negative occurrence differences concentrated in South Asia, South Africa and South America (blue bars), in contrast with North Asia, East Europe, North America and Antarctic (red bars). The larger part of the excluded locations are located in the transition between positive and negative difference zones (e.g. North and West Europe and Middle Asia). Observing the occurrence time differences versus latitude, it was observed some pattern: most of the locations that are between 40°N and -40°S show negative Δt_0 ($t_E < t_I$, see Figure 8A). For higher latitudes than 40°N or lower than -40°S , in most of the locations the occurrence time was detected first in CORE then COEI (positive Δt_0 ; $t_E > t_I$).

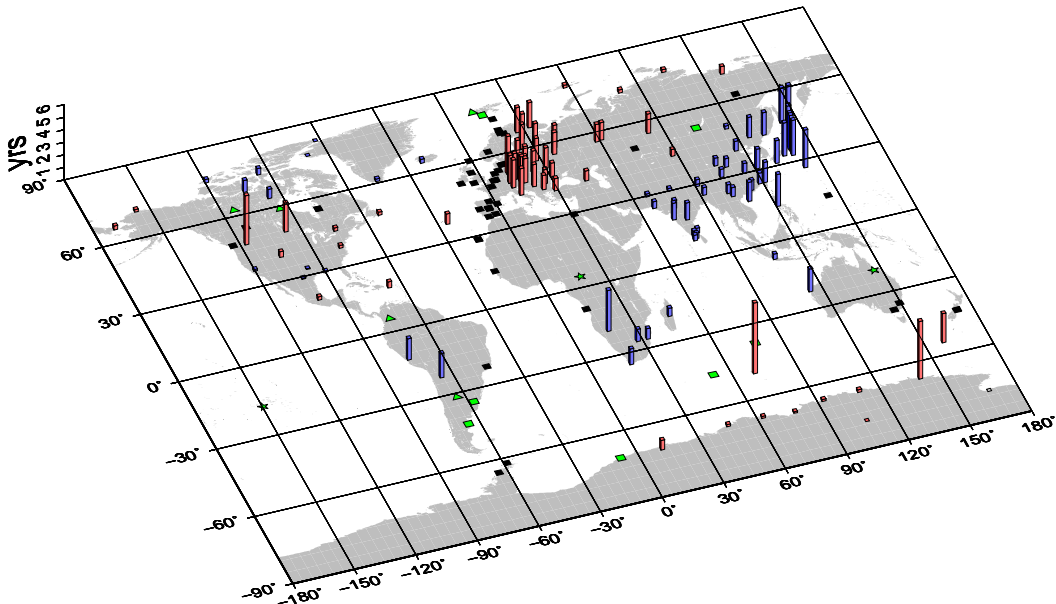


Figure 5: Global distribution of the comparison between the 1969 jerk detection in X component in CORE and COEI datasets for the 186 observatory locations studied. The bars in the map represent the occurrence time difference Δt_0 (see Equation 3). Red bars for positive differences ($t_E > t_I$), blue bars for negative differences ($t_E < t_I$) and gray squares for zero difference. Also, The map shows the locations where the jerk was excluded in CORE (black stars), in COEI (black squares) and both data sets (black triangle). Locations where the jerk was not detected in CORE (green stars), in COEI (green squares) and both data sets (green triangles) are exhibit too.

In average, error bars of COEI increased their value by 55% (Table 1), as expected due to the influence of external fields. Comparing the mean error bars of COEI (-0.30 and 0.35) and the observatory data results we found that the real data showed a much higher value of -1,5 and +1,9. This fact demonstrates how using a model as CM4 is a simplification and generates a smoother version of the real data. Another relevant characteristic is that the error bars are approximately symmetric in CORE and COEI datasets, differently from the results found in real observatory data that are mostly not-symmetric (Pinheiro *et al.*, 2011).

5.1.2 1978 Geomagnetic Jerk (X component)

The 1978 jerk was detected in CORE (X component) in 72% of the locations while in COEI dataset it was identified only in 50% (Table 1). This jerk was detected in 43% of the locations in both datasets. The 1978 jerk showed a larger number of excluded locations compared to the 1969 jerk. A similar behavior was noted in the observatory data results (Pinheiro *et al.*, 2011) where the X component of the 1978 jerk presented 67 excluded locations.

The absolute mean difference of $|\Delta t_0| = 0.63$ years indicate that this event do not shows high difference contrast. In general, external fields (in COEI) tended to delay the 1978 jerk detection, since 77,5% of the locations had negative Δt_0 . The mean occurrence time in COEI differed by 1.04 years (Table 1) compared to CORE. This happens because in 11 locations where the 1978 jerk was excluded (e.g. Borok observatory location, BOX, Russia) and two where it was not detected (e.g. Pleshentzi (Minsk) observatory location, MNK, Belarus) in CORE dataset, this jerk was detected in COEI dataset at the extreme of the detection time window (1982), increasing the mean occurrence time.

The higher time occurrence difference values are located between 45°N and -45°S. The global distribution of the differences (Figure 6) evidence its mainly negative tendency concentrated in South and Middle Asia (blue bars).

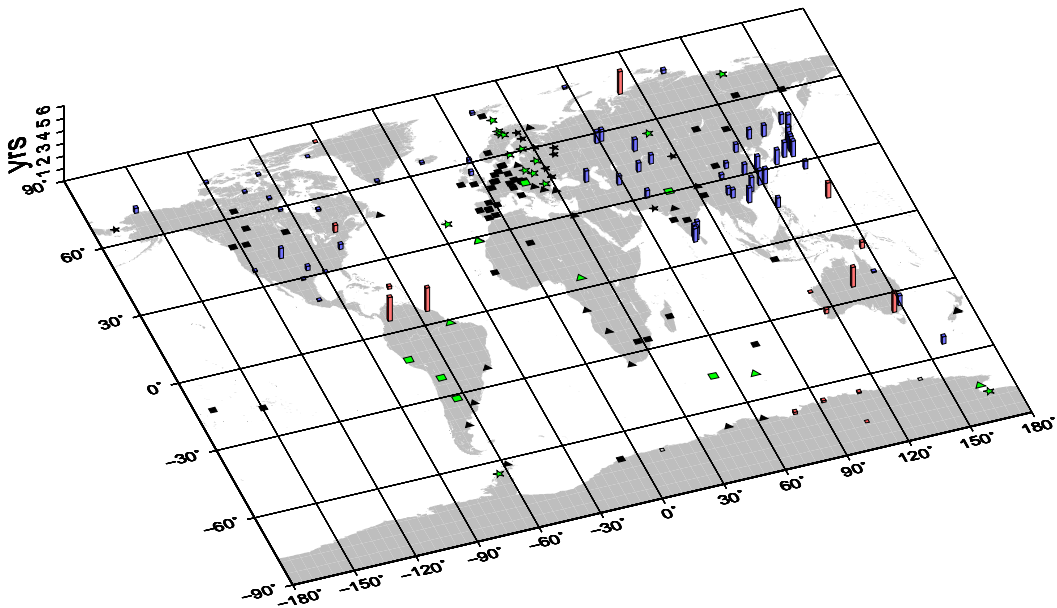


Figure 6: Global distribution of the comparison between the 1978 jerk detection in X component in CORE and COEI datasets for the 186 observatory locations studied. The labeling scheme is the same as in Figure 5.

Analyzing the occurrence time differences versus latitude (Figure 7B), we noted that the X component showed an equatorial pattern with a mainly negative Δt_0 in the Northern Hemisphere and mainly positive Δt_0 in the Southern Hemisphere.

The X component of the 1978 jerk showed a different behavior than the same component for the 1969 jerk: an increase in the error bars and a larger number of excluded locations. Moreover, the mean absolute occurrence time difference $|\Delta t_0|$ is smaller than in the 1969 jerk. The minimum and maximum error bars showed mean increase of 0.49 years and 0.53 years, respectively. These increases represent 72% of the CORE error bars (Table 1). In the 1978 jerk, external fields affected mostly the error bars than the occurrence times. Comparing the mean error bars of COEI and the observatory data results, the real data showed a larger value of -1,7 and +1,7 and also a symmetric behavior, in this case.

5.1.3 1991 Geomagnetic Jerk (X component)

In the CORE dataset, the 1991 jerk (X component) was detected in 80% of the chosen locations, while in COEI dataset it was identified in only in 36%. This occurred due to the largest number of excluded locations (58%) compared to all other jerks and components (See Table 1). This jerk was identified in only 66 locations in both datasets.

The mean occurrence time \bar{t}_0 in the two datasets did not exhibit a appreciable difference, considering the mean error bars (Table 1). The mean occurrence time from observatory data results in Pinheiro *et al.* (2011) was detected before than COEI with a difference of 0.97 years. Half of the locations where this jerk was detected in both datasets showed negative Δt_0 and the other half, positive Δt_0 . These results showed no preferential tendency to delay or to anticipate the 1978 jerk in COEI dataset. However, a significant absolute mean difference of 1.34 years caused by external influences was found. Some individual locations exhibited large difference value. Stennis Space Centre location observatory (Bay St. Louis BSL, United States) presented the largest value of -6.01 years.

Figure 7 shows a great contrast between negative differences (blue bars mainly located in Middle Asia and Antarctic) and positive differences (red bars mainly located in North America, South Africa and East Asia). A larger quantity of excluded locations was concentrated in Europe and South-East Asia. When these results were compared with those obtained in real data (Figure 7 on Pinheiro *et al.*, 2011), we noted similar excluded locations, positive and negative geographical patterns. The X component of the 1991 jerk showed a latitudinal pattern for Δt_0 negative differences in higher latitudes than 40°N and positive differences in lower latitudes with the exceptions of FRD, DAL, BSL and DLR observatory locations which are the largest negative differences identified in this event. Southern Hemisphere presented negative Δt_0 near the Equator, and positive Δt_0 in latitudes lower than -40°S (Figure 8C).

Most of locations increased their error bars with the addition of external field. The mean error bars for the 1991 jerk (X component) doubled its value with the addition of external fields (Table 1). This demonstrates that the influence of magnetospheric and ionospheric field are significantly in this case. The number of excluded locations and the error bars of the X component (1991 jerk) are in general larger than in the 1969 and 1978 jerks.

5.2 Y Field Component

5.2.1 1969 Geomagnetic Jerk (Y component)

The Y component is known to be the less affected by external fields because of the smaller influence of ring currents (see Figure 10C and 10D). The 1969 jerk was detected in the same number of places for CORE and COEI (175 locations, see Table 2) but not in the same locations. In both dataset this jerk was detected in only 171 locations. Holme and de Viron (2005) have argued the existence of a direct connection between geomagnetic jerks occurrence times and variations in changes of the length-of-day (LOD). Considering that jerks and LOD may originate primarily from torsional oscillations, jerks should be better observable in a component which is approximately parallel to these motions (Y component) than others (X and Z components).

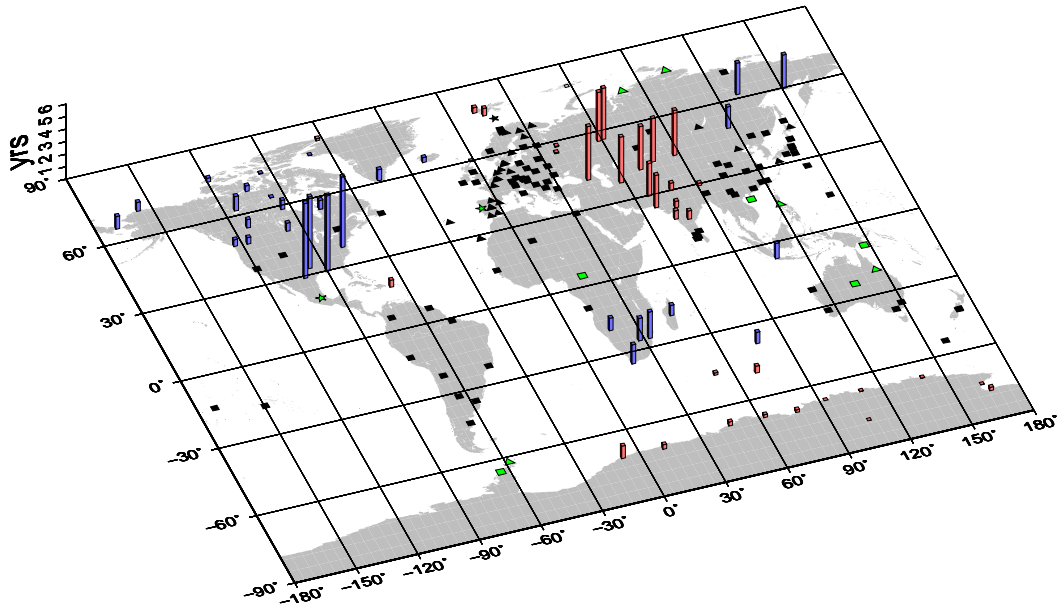


Figure 7: Global distribution of the comparison between the 1991 jerk detection in X component in CORE and COEI datasets for the 186 observatory locations studied. The labeling scheme is the same as in Figure 5.

The mean occurrence time \bar{t}_0 in the two model datasets are very similar (Table 2) and not different from the real data results (1969.83). The occurrence time differences exhibited no preferential tendency to delay or to anticipate the jerk since the number of locations with positive or negative differences are similar. The small absolute difference of 0.13 years in both datasets demonstrated that most differences have low values and they are not significant, considering the main error bars. The higher occurrence time difference of 2.05 years was founded in Sao Miguel observatory location (SMG, Portugal, Figure 9A and 9B).

The global distribution of the differences (Figure 10) indicates that even though in the Northern Hemisphere these differences are positive, there are negative differences concentrated in the North and West Europe (in the same zone where we found the main part of excluded locations in X component) and in the most of Southern Hemisphere. Latitudinally, the 1969 jerk (Y component) showed an equatorial contrast: most of the locations in Northern Hemisphere presented a positive Δt_0 , while most of locations in South Hemisphere present a negative Δt_0 (see Figure 13A).

Table 2: Jerk detection for CORE and COEI model datasets in the Y component of the 1969, 1978 and 1991 geomagnetic jerk. The labeling scheme is the same as in Table 1.

| Jerk | Dataset | DET | EXC | NOT | \bar{t}_0 | \bar{e}_{min} | \bar{e}_{max} |
|------|---------|-----|-----|-----|-------------|-----------------|-----------------|
| 1969 | CORE | 175 | 7 | 4 | 1970.31 | -0.43 | 0.44 |
| | COEI | 175 | 9 | 2 | 1970.27 | -0.48 | 0.49 |
| 1978 | CORE | 176 | 6 | 4 | 1978.25 | -0.59 | 0.57 |
| | COEI | 172 | 9 | 5 | 1978.21 | -0.58 | 0.58 |
| 1991 | CORE | 154 | 24 | 6 | 1991.44 | -0.63 | 0.63 |
| | COEI | 147 | 27 | 7 | 1991.44 | -0.66 | 0.67 |

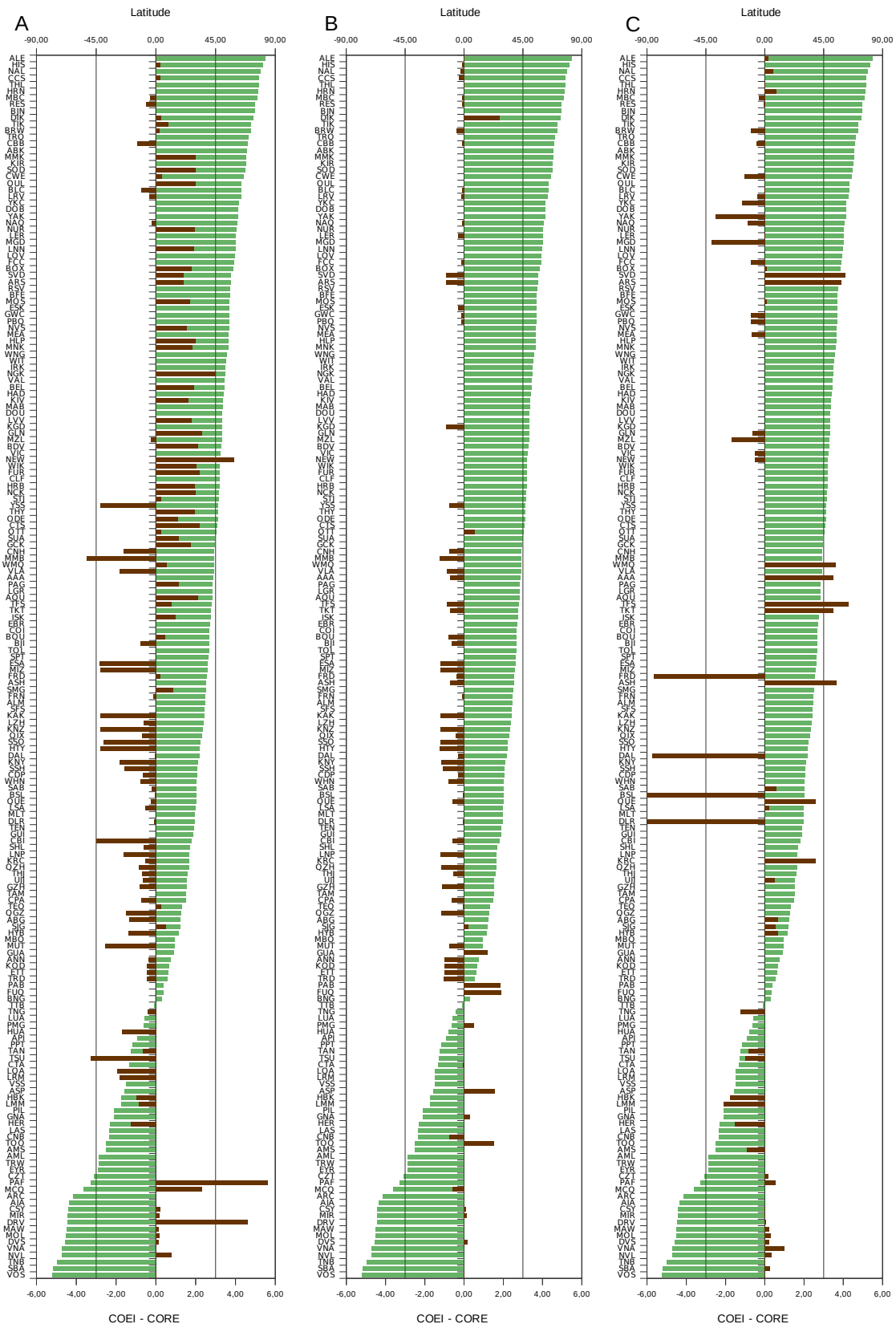


Figure 8: Differences on the occurrence times of COEI and CORE datasets (Δt_0), represented by the red bars (bottom scale), plotted versus latitude (blue bars, top scale) for the locations (left scale) where the (A) 1969, (B) 1978 and (C) 1991 jerks was detected in both datasets in X component.

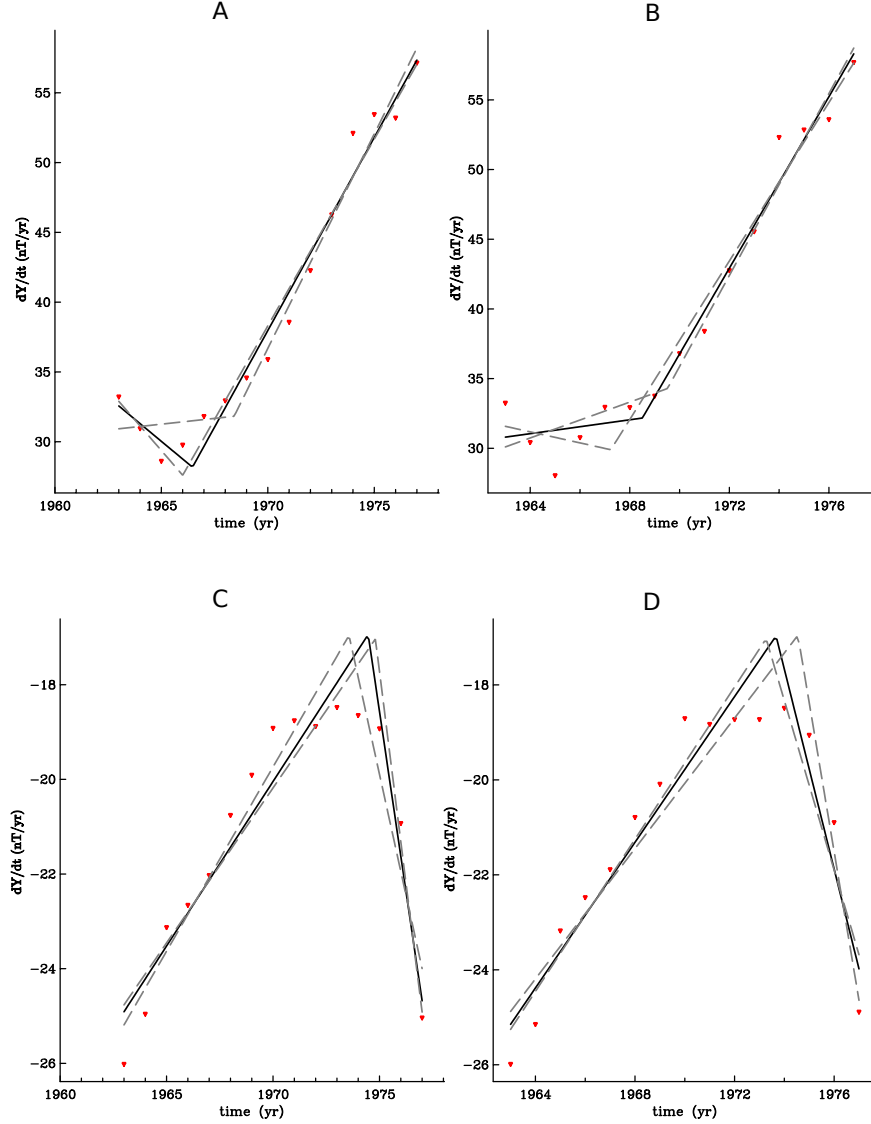


Figure 9: Detection of 1969 jerk in the Y component in: Sao Miguel Observatory (SMG, Portugal) location in (A) CORE and (B) COEI datasets. The detected jerk has positive amplitude (V-shaped form). The detection date for (A) CORE was 1966.46 and for (B) COEI was 1968.51. Another example is in Vemadsky observatory (AIA, Antarctic) location in (C) CORE and (D) COEI datasets. The detected jerk in this location presents a negative amplitude (inverted V-shaped form). The detection date for (A) CORE was 1974.47 and for (B) COEI was 1973.67. The external influences produce a difference in the occurrence time between CORE and COEI data sets: positive difference ($t_E > t_I$) in A/B and negative difference ($t_E < t_I$) in C/D.

Observe that, as expected in model data, the error bars did not vary significantly from CORE to COEI in the Y component (-0.06 and 0.05 years). Moreover, these error bars are smaller than the real data results. It is important to note that Y component error bars are smaller than X component error bars even in the CORE dataset. This fact indicates that jerks are better detected in the Y component not only because of the ring current influence but also due to the natural jerk morphology.

5.2.2 1978 Geomagnetic Jerk (Y component)

The small difference between the number of detected locations in CORE and COEI datasets for the 1978 jerk (only 4, see Table 2) confirmed the small influence of external fields in the Y component. This jerk was identified in 170 locations in both CORE and COEI datasets.

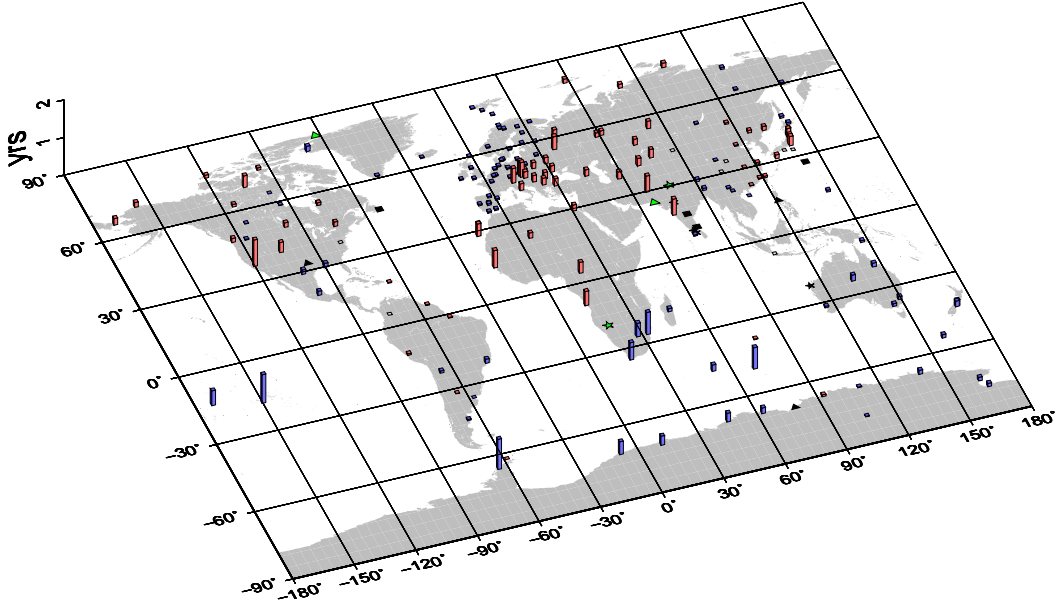


Figure 10: Global distribution of the comparison between the 1969 jerk detection in Y component in CORE and COEI datasets for the 186 observatory locations studied. The labeling scheme is the same as in Figure 5.

The mean occurrence time \bar{t}_0 of the detected jerk in CORE and COEI datasets and in observatory data (1978.20) are similar. Most of locations showed negative occurrence time differences Δt_0 but some large differences are found in locations with positive Δt_0 . For example, the occurrence time difference in Esashi observatory location (ESA, Japan) is 0.80 years, a high value for the Y component.

Geographically, the most negative difference values are concentrated in Europe and South Asia and the most positive values are concentrated in Middle and East Asia. Other smaller values (negative and positive) are widely distributed (Figure 11). In Figure 13B there is a clear tendency to negative differences Δt_0 in all latitudes with higher values in latitudes between 45°N and 40°N and near to the Equator in the Northern Hemisphere, while in the Southern Hemisphere presents lower values mainly negative. Some locations with positive Δt_0 were founded between 40°N and -40°S .

The error bars did not increase significantly from CORE to COEI (only 5% in average). The mean error bars of COEI are much smaller than observatory error bars (-1,2 and 1,1) for the Y component of the 1978 jerk. The three datasets (CORE, COEI and observatory) share a common characteristic that is approximately symmetric error bars.

5.2.3 1991 Geomagnetic Jerk (Y component)

The 1991 jerk was detected in 154 locations in CORE and 147 locations in COEI dataset (Table 2). This jerk was the worst detected in Y component with a detection of 79% of locations compared with the 92% and 91% of the 1969 and 1978 jerk detections, respectively. It was detected in CORE and COEI in 147 locations.

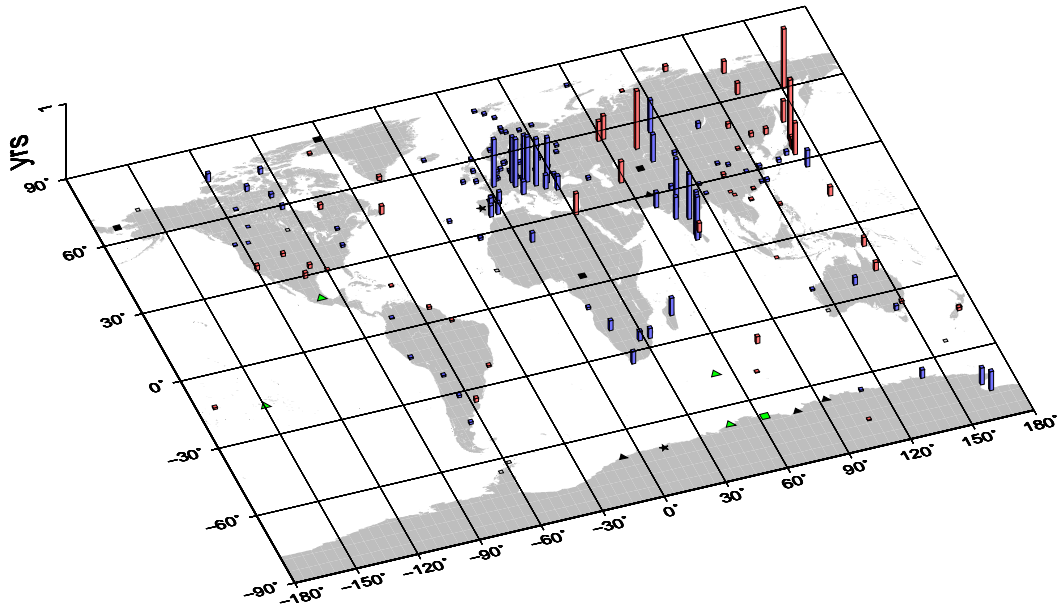


Figure 11: Global distribution of the comparison between the 1978 jerk detection in Y component in CORE and COEI datasets for the 186 observatory locations studied. The labeling scheme is the same as in Figure 5.

Although, the mean occurrence time \bar{t}_0 in the two model datasets are practically the same (Table 2) and the difference from the observatory data results is small (1991.26), the mean absolute occurrence time difference between both model datasets is the largest of the three jerks ($|\Delta t_0| = 0.24$ years). The occurrence time differences (Δt_0) founded are mainly positive ($\Delta t_0 > 0$). This result could show that, in general, jerks were preferentially anticipated in COEI dataset for the 1991 jerk. Large differences in individual locations were identified. For example, Neumayer Station III observatory location (VNA, Antarctic) presented a difference of -1.49 years.

High positive differences were founded in East Europe, contrast with lower values of differences founded in Middle Asia and Antarctic (Figure 12). Similar to the 1969 jerk, the 1991 jerk showed an equatorial contrast for the occurrence time differences Δt_0 (Figure 13C). In Northern Hemisphere most of locations presents a positive Δt_0 with larger values in high latitudes which decrease with the latitude, while most of locations in South Hemisphere present a negative Δt_0 .

Besides, the 1991 jerk showed the largest error bars in both datasets, they did not vary significantly from CORE to COEI in the Y component (-0.03 and 0.04 years). Moreover, these error bars are smaller than the real data results, as expected in model data.

5.3 Z Component

5.3.1 1969 Geomagnetic Jerk (Z component)

The detection of jerks in the Z component is usually more difficult than in X and Y. This happens because additionally to the external fields, Z component is influenced by induced currents in the crust and in the oceans. In the CORE dataset, the 1969 jerk was detected in 81% and not detected in 10% of the studied locations. In COEI the jerk was detected in 79% of locations and not detected in 9% (Table 3). In both CORE and COEI datasets, this jerk was detected at 145 locations.

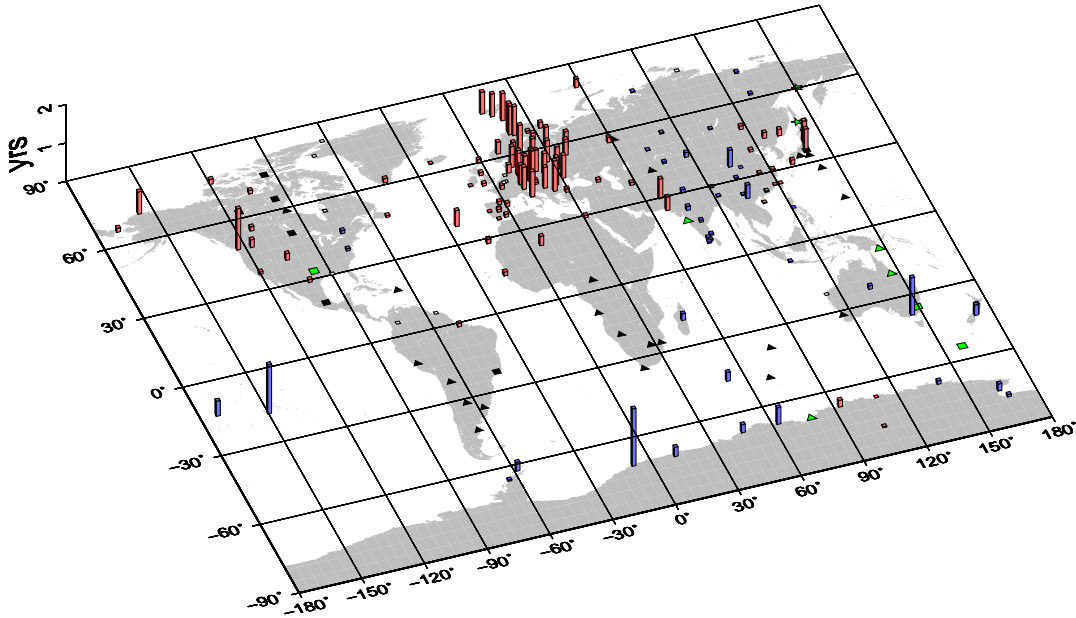


Figure 12: Global distribution of the comparison between the 1991 jerk detection in Y component in CORE and COEI datasets for the 186 observatory locations studied. The bars in the map represent the occurrence time difference Δt_0 . The labeling scheme is the same as in Figure 5.

In this model data, Z component showed a similar behavior to Y component like high number of locations detected, small occurrence time differences and low error bars. This behavior is not coherent with the results in observatory data, as presented in Pinheiro *et al.* (2011) where Z component showed more resemblance with X component. The mean occurrence time \bar{t}_0 in the two model datasets are similar and the difference between them and the real data results is small (1970.62).

Similar number of locations with positive occurrence time differences ($\Delta t_0 > 0$) and locations with negative occurrence time differences ($\Delta t_0 < 0$) shows that, in general, jerks were not preferentially anticipated or delayed in COEI dataset for the 1969 jerk in this component. The absolute occurrence time founded $|\Delta t_0| = 0.25$ years reveals that the difference values are mostly lower but some individual locations exhibit higher values, e.g. Krasnaya Pakhra (Moscow) observatory location (MOS, Russia) with the largest occurrence time difference value of 2.07 years.

Table 3: Jerk detection for CORE and COEI model data in the Z component of the 1969, 1978 and 1991 geomagnetic jerk. The labeling scheme is the same as in Table 1.

| Jerk | Dataset | DET | EXC | NOT | \bar{t}_0 | \bar{e}_{min} | \bar{e}_{max} |
|------|---------|-----|-----|-----|-------------|-----------------|-----------------|
| 1969 | CORE | 151 | 16 | 19 | 1970.50 | -0.53 | 0.57 |
| | COEI | 147 | 22 | 17 | 1970.40 | -0.64 | 0.62 |
| 1978 | CORE | 142 | 33 | 11 | 1977.62 | -0.63 | 0.66 |
| | COEI | 138 | 35 | 13 | 1977.53 | -0.77 | 0.68 |
| 1991 | CORE | 139 | 38 | 6 | 1992,11 | -0.67 | 0.67 |
| | COEI | 126 | 49 | 8 | 1992,10 | -0.76 | 0.74 |

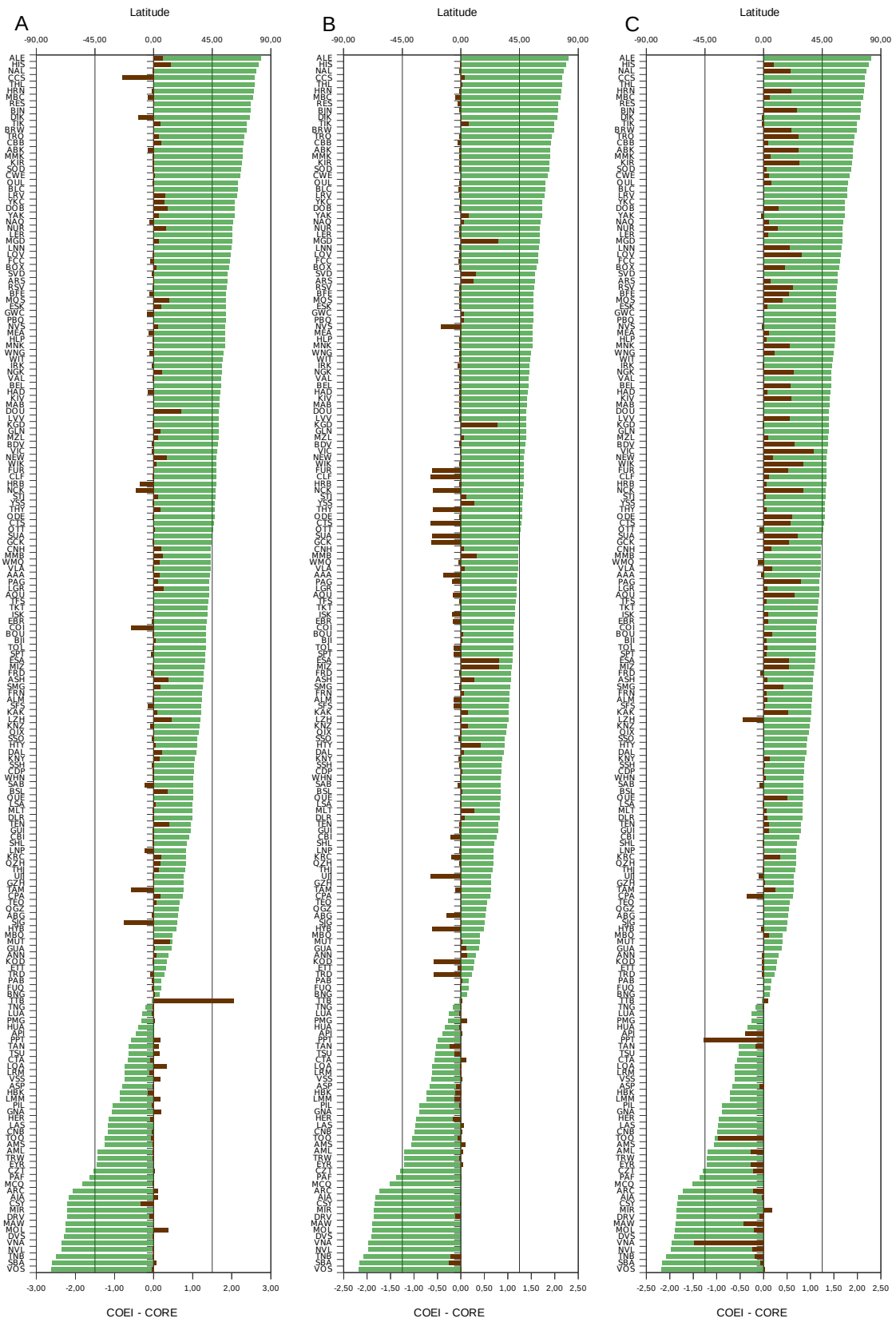


Figure 13: Differences on the occurrence times of COEI and CORE datasets (Δt_0), represented by the red bars (bottom scale), plotted versus latitude (blue bars, top scale) for the locations (left scale) where the (A) 1969, (B) 1978 and (C) 1991 jerks was detected in both datasets in Y component.

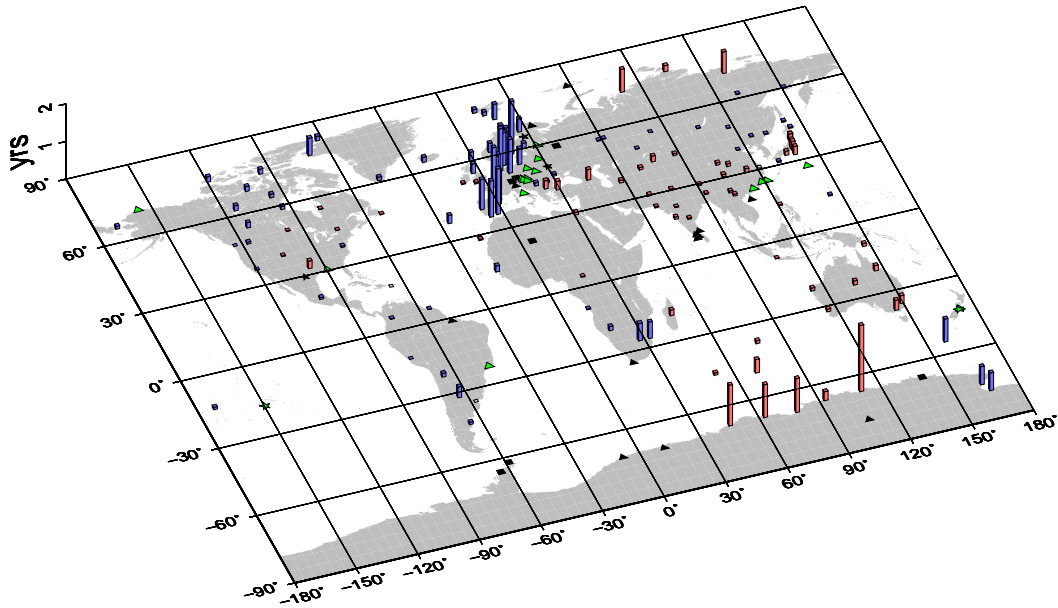


Figure 14: Global distribution of the comparison between the 1969 jerk detection in Z component in CORE and COEI datasets for the 186 observatory locations studied. The labeling scheme is the same as in Figure 5.

In the Figure 14, the global distribution of the differences showed that the larger differences are located in the East Europe (negative Δt_0) and Antarctic (positive Δt_0). An interesting feature is that the differences present a longitudinal pattern: positive differences between -180°W to 30°E and negative differences between 30°E to 180°E . The larger negative differences are concentrated in approximately the same zone where we found the main part of excluded locations in X component (East Europe) and the main part of the not detected and excluded locations in Z component are concentrated in approximately the same zone of the large positive differences of X component. Observing the occurrence time differences versus latitude, we noted that most locations in Northern Hemisphere present negative occurrence time differences with larger values in latitudes between 40°N and 50°N . In the Southern Hemisphere, locations show mainly positive occurrence time differences with a clear tendency to increase while the latitude is lowest (see Figure 17A).

The minimum and maximum error bars of COEI increased their value in 28% and 12% respectively, due to the influence of external fields. The observatory data results showed much higher values (-1.5 and 1.3) of error bars. This fact demonstrated that the Z component is influenced not only by external fields, in real data. Possibly the influence of the induced field

5.3.2 1978 Geomagnetic Jerk (Z component)

In the CORE dataset, the 1978 jerk was detected in 76% of the locations in Z component. With the addition of external fields (COEI dataset), the 1978 jerk (Z component) was detected in 74% of the chosen locations. It was detected in both datasets in 135 locations (Table 3).

The mean occurrence time \bar{t}_0 in the two model datasets are similar between them and with the real data results (1977.04). The number of locations with positive occurrence time differences Δt_0 is slightly greater than locations with negative occurrence time differences Δt_0 . This result evidences a small delay of the 1978 jerk in the COEI dataset but, considering the mean error bars, this delay is not significant.

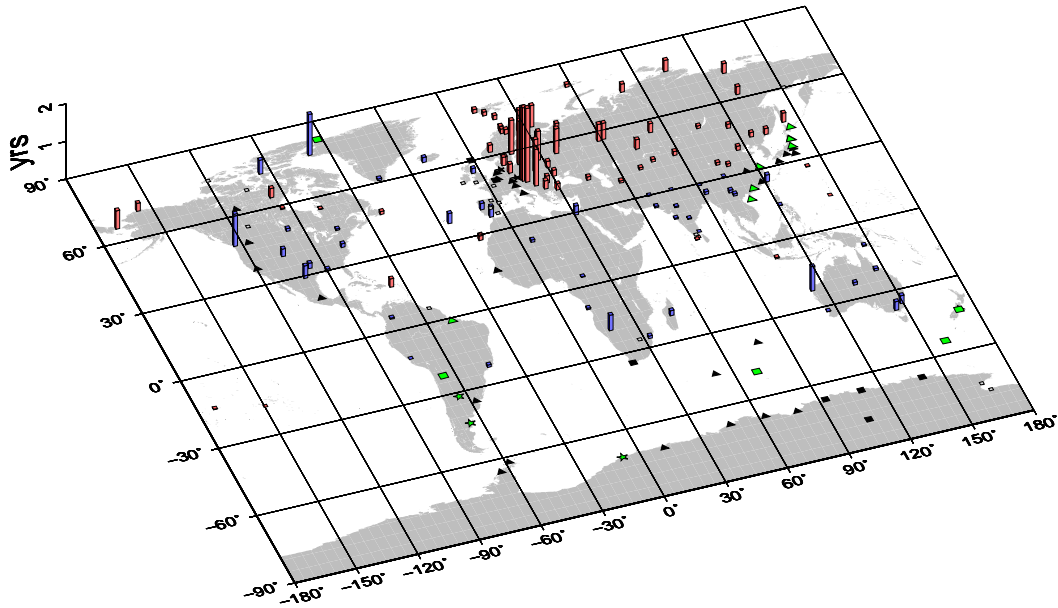


Figure 15: Global distribution of the comparison between the 1978 jerk detection in Z component in CORE and COEI datasets for the 186 observatory locations studied. The labeling scheme is the same as in Figure 5.

The absolute mean occurrence time difference $|\Delta t_0| = 0.27$ years proves this fact. However, some locations with larger difference values were found, for example Tihany observatory location (THY, Hungary) where the occurrence time difference was 1.96 years.

Mainly positive differences were founded in East Europe (high values) and North and Middle Asia (lower values). Negative values can be founded in North America, South Asia and Africa (Figure 15). Figure 17B shows that Z component has a clear tendency to positive differences Δt_0 in the North Hemisphere. These values are increasing while the latitude is decreasing to the maximum difference value in 45°N , then these values are decreasing together with latitude to the equator. In South Hemisphere the tendency changes to lower values mainly negative.

The influence of external fields increased the error bars in COEI in -0.12 and 0.03 years. Real data showed a much higher value of -1,8 and +1,6 compared with the mean error bars of COEI. The error bars are not-symmetric in CORE and COEI datasets, similarly from the results found in real observatory data (Pinheiro *et al.* 2011).

5.3.3 1991 Geomagnetic Jerk (Z component)

In the Z component, the 1991 jerk was detected in 74% of the locations in CORE dataset. In COEI, the jerk was detected in 67.7% of the studied locations. In 126 observatory locations this jerk was identified in both datasets (Table 3).

As well as Y component, the mean occurrence times \bar{t}_0 are similar in both datasets. This behavior was observed in all jerks in Z component. A similar number of locations with positive occurrence time differences ($\Delta t_0 > 0$) and locations with negative occurrence time differences ($\Delta t_0 < 0$) were identified. This result shows that, in general, jerks were not preferentially anticipated or delayed in COEI dataset for the 1991 jerk in this component.

The absolute mean difference $|\Delta t_0| = 0.18$ years shows that, in general, the difference values are low but some locations with higher values like the 1.90 years difference of Kiruna observatory location (KIR, Sweden) were found.

The geographical distribution of the differences showed a interesting longitudinal pattern, the negative differences are located in North and East Europe, Middle and South Asia and North Africa. Otherwise, negative differences (which shows lower values) were founded in North and South America and East Asia (Figure 16). The 1991 jerk detection revealed a similar equatorial contrast as the 1978 jerk (Z component) with larger difference values Δt_0 mainly positive in higher latitudes, decreasing together the latitude and a South Hemisphere showed difference values Δt_0 mainly negative (Figure 17C).

In average, error bars of COEI increased their value by 15% due to the influence of external fields. The error bars are approximately symmetric in CORE and COEI datasets. Comparing the mean error bars of COEI and the observatory data results, we found that the real data showed a much higher value of -1,5 and +1,9 and they are mostly non-symmetric (Pinheiro et al., 2011) differently from the model data results.

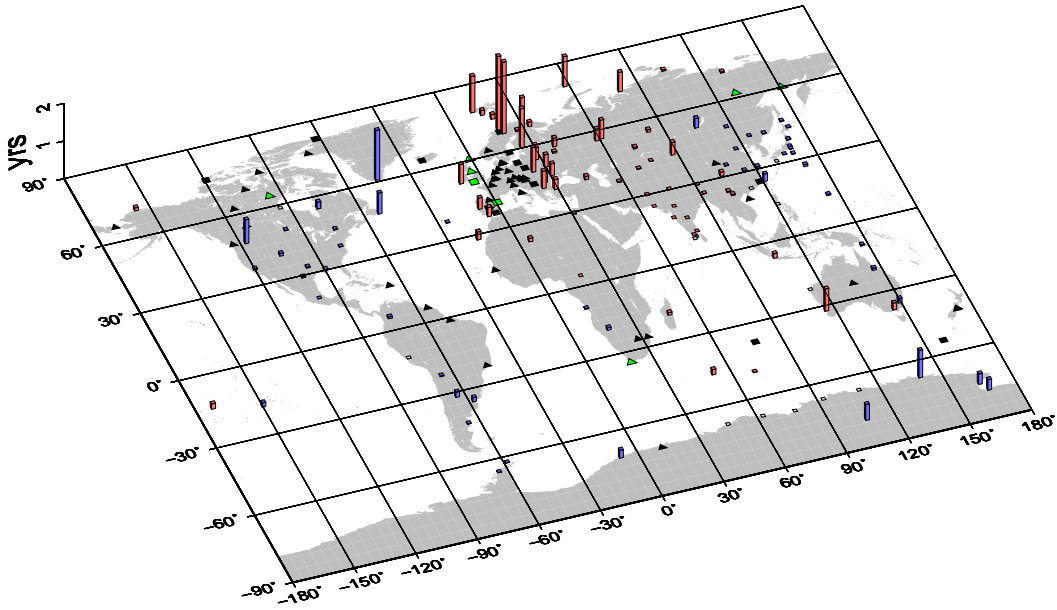


Figure 16: Global distribution of the comparison between the 1991 jerk detection in Z component in CORE and COEI datasets for the 186 observatory locations studied. The bars in the map represent the occurrence time difference Δt_0 . The labeling scheme is the same as in Figure 5.

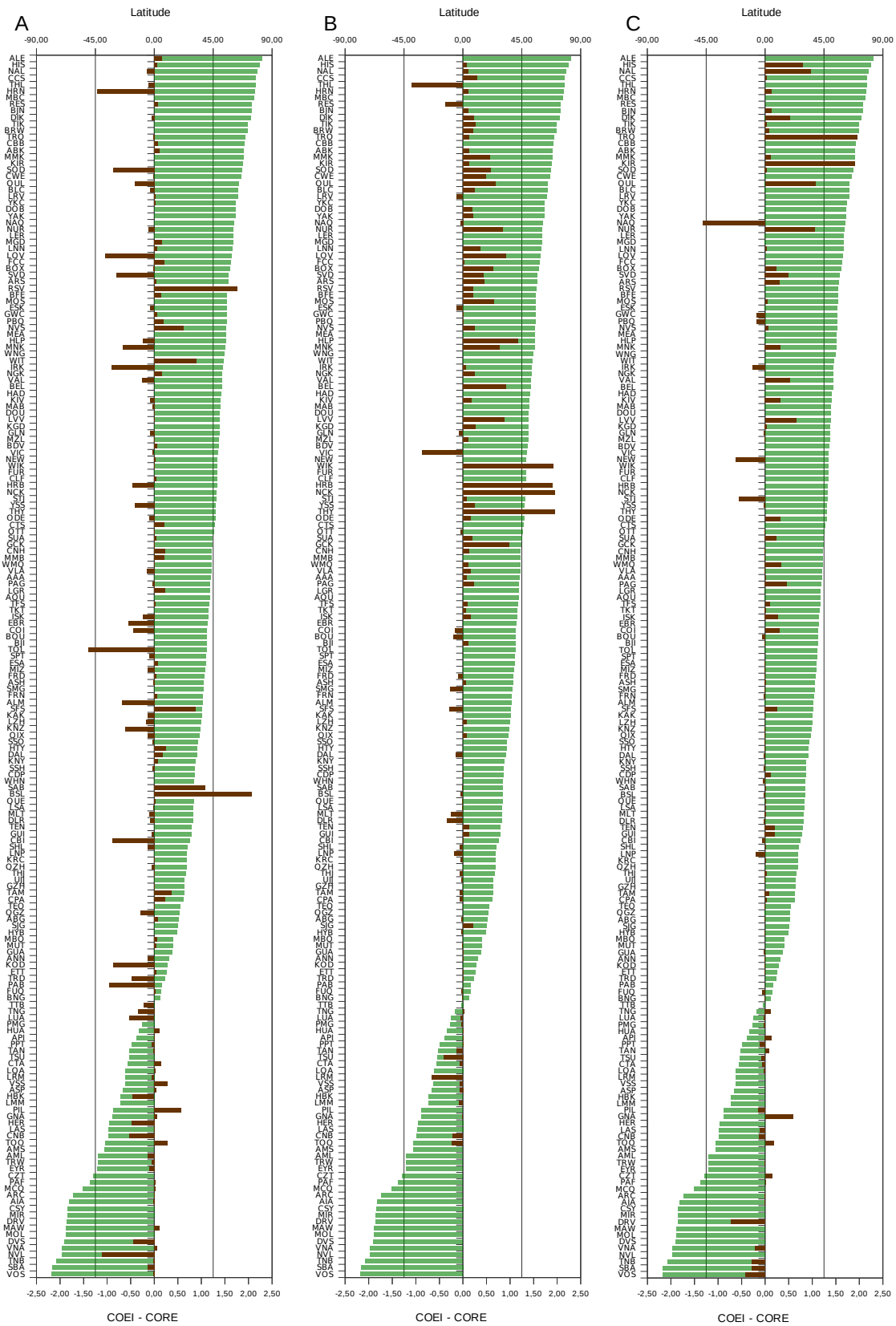


Figure 17: Differences on the occurrence times of COEI and CORE datasets (Δt_0), represented by the red bars (bottom scale), plotted versus latitude (blue bars, top scale) for the locations (left scale) where the (A) 1969, (B) 1978 and (C) 1991 jerks was detected in both datasets in Z component.

6 Conclusions

The fitting of two straight line segments to the secular variation is a simple detection method that allows the calculation of error bars on the occurrence time and amplitude of geomagnetic jerks. The ability of the CM4 field model to separate internal and external fields was used in this work to investigate the 1969, 1978 and 1991 jerks (X, Y and Z components) in the core field (CORE dataset), and in the core field added to external and induced contributions (COEI dataset).

Since geomagnetic jerks have an internal origin, they should be most easily detected in the core field data. As expected, the studied jerks were best identified in CORE dataset for all components. Although, the variation of the detected dates and error bars was not the same for each jerk and magnetic field component. The largest number of locations where the jerks were observed, both in COEI and CORE datasets, was in East (Y) component. As geomagnetic jerks may originate from torsional oscillations they should be better observable in a component which is approximately parallel to these motions (Y component) than others (X and Z components). This result evidences that the difficulty to detect main field features, such as jerks, in X and Z components is not only due to the external influences.

It is well known that the external fields disturb the main field signal and subsequently may disturb jerks detection. The reduction of jerk detection in the model COEI dataset, in most jerks and components, demonstrates this fact. In this work, it was evidenced that the detection of jerks in the X and Z components were more affected by external influences. This result is consistent with observatory data results. Moreover, there were events where the addition of external fields allowed the detection of jerks that had not been detected in CORE dataset. In these few cases, linear trends may be considerably modified by the external field signals, producing jerk-like artefacts. This result showed that it is possible to detect V-shaped features in the secular variation data, not caused by the core field, but produced by external magnetic fields. It is possible that other influences, such as noise and outliers, may affect observatory data and induce detection of jerk-like features.

An important characteristic of the geomagnetic jerks is their non-simultaneous behavior at the Earth's surface. Jerk characteristics, such as differential delays, have been used in attempts to obtain information about mantle electrical conductivity. The occurrence time differences Δt_0 calculated for jerks detected in both datasets, evidenced that a jerk could be detected apparently earlier (when the difference is negative $t_E < t_I$) or later (when the difference is positive $t_E > t_I$) in the records, due to external fields influence. The patterns of early/late 1969, 1978 and 1991 jerks for the X component in observatory data from Pinheiro *et al.* (2011) are similar to the difference patterns between CORE and COEI. This is a pertinent result for studies involving jerks differential delays that may be cause not only by jerks dynamics or mantle conductivity, but by external field artefacts. The absolute values of these differences $|\Delta t_0|$ revealed large differences in individual locations of the order of 6.01 years, mainly in the X component demonstrating how important is to consider the influence of external field in jerk detection studies.

The error bars in the jerk occurrence times also indicated the influence of external fields on the secular variation series. The error bars in CORE dataset are considered as the natural error produced by the internal field and by the chosen simple detection method, used in this work. When jerks were detected in COEI dataset, the error bars increased their values, compared to CORE dataset. In general, the larger error bars were found in the X and Z components, and smaller in the Y component. Comparing our results with observatory data, the largest differences are found in the 1969 and 1978 jerks, especially for the Y and Z components. In these cases, the error bars of observatory data are roughly the double of error bars in COEI dataset. For the 1991 jerk, these differences between COEI and real data are smaller, about 30%. Another relevant characteristic is that the error bars are approximately symmetric in CORE and COEI datasets, differently from the results found in real observatory data that are mostly non-symmetric. These results demonstrated how using a model as CM4 is a simplification and smoother version of the real data.

External and induced fields are sources of the geomagnetic field that may influence the secular variation time series, even considering annual means data. This work proposes that, before analyzing geomagnetic jerks in annual means data, it is necessary to extract the maximum as possible the external and induced fields. A better understanding of external and induced fields may contribute

to studies involving the non-simultaneous behavior of jerks and therefore, the estimates on mantle electrical conductivity and dynamical nature of geomagnetic jerks.

7 References

- Alexandrescu, M., Gilbert, D., Hulot, G., Mouël, J., Saracco, G., 1995. Detection of geomagnetic jerks using wavelet analysis. *J. Geophys. Res.* 100: 12557-12572.
- Alexandrescu, M., Gibert, D., Hulot, G., Mouël, J., Saracco, G., 1996. Worldwide wavelet analysis of geomagnetic jerks. *J. Geophys. Res.* 101, 21975–21994.
- Allredge, L., 1977. Deep mantle conductivity, *J. Geophys. Res.*, 82(33), 5427–5431.
- Allredge, L., 1984. A discussion of impulses and jerks in the geomagnetic field. *J. Geophys. Res.* 89: 4403-4412.
- Bloxham, J., Zatman, S., Dumberry, M., 2002. The origin of geomagnetic jerks, *Nature*, 420, 65–68.
- Courtillot, V., Ducruix, J., Le Mouël, J., 1978. Sur une accélération récente de la cariatioséculaire du champ magnétique terrestre. *C. R. Acad. Sci. Paris, Ser. D* **287**: 1095-1098.
- Chulliat, A., Thébault, E., Hulot, G., 2010. Core field acceleration pulse as a common cause of the 2003 and 2007 geomagnetic jerks, *Geophys. Res. Lett.*, **37**, L07301, doi:10.1029/2009GL042019.
- De Michelis, P., Cafarella, L., Meloni, A., 2000. A global analysis of the 1991 geomagnetic jerk, *Geophys. J. Int.*, **143**, 545–556.
- De Michelis, P., Tozzi, R., 2005. A local intermittency measure (LIM) approach to the detection of geomagnetic jerks, *Earth Planet. Sci. Lett.*, **235**, 261–272.
- Holme, R., De Viron, O., 2005. Geomagnetic jerks and a high-resolution length-of-day profile for core studies, *Geophys. J. Int.* (2005) **160** (2): 435-439. doi: 10.1111/j.1365-246X.2004.02510.
- Le, G., Cai, Z., Wang, H., Zhu, Y., 2012. Solar cycle distribution of great geomagnetic storms, *Astrophys Space Sci* **339**:151–156 DOI 10.1007/s10509-011-0960-y
- Le Huy, M., Alexandrescu, M., Hulot, G., Le Mouël, J. 1998. On the characteristics of successive geomagnetic jerks. *Earth Planets Space* **50**: 723-732.
- Le Mouël, J., Ducruix, J., Duyen, C., 1982. The worldwide character of the 1969–1970 impulse of the secular acceleration rate, *Phys. Earth Planet. Inter.*, **28**, 337–350.
- Malin, S., and B. M. Hodder, 1982. Was the 1970 geomagnetic jerk of internal or external origin?, *Nature*, 296, 726–728.
- Malin, S., Hodder, B., Barraclough, D., 1983. Geomagnetic secular variation: a jerk in 1970, in *75th Anniversary Volume of Ebro Observatory*, ed. by J.R. Cardus (Ebro Observatory, Tarragona, 1983), pp. 239–256.
- Mandea, M., Macmillan, S., 2000. International Geomagnetic Reference Field—the eighth generation. *Earth Planets Space* **52**, 1119–1124.
- Mandea, M. et al. (06 co-authors), 2010. Geomagnetic jerks: rapid core field variations and core dynamics. *Space Science Review*, **155**: 147-175.
- Nagao, H., Iyemori, T., Higuchi, T., Araki, T., 2003. Lower mantle conductivity anomalies estimated from geomagnetic jerks. *J. Geophys. Res.* **108**.
- Olsen, N., 1998. The electrical conductivity of the mantle beneath Europe derived from C-responses from 3 to 720 h. *Geophys. J. Int.* **133**, 298–308.
- Olsen, N., Mandea, M., 2007. Investigation of a secular variation impulse using satellite data: The 2003 geomagnetic jerk, *Earth Planets Space*, **255**, 94–105.
- Olsen, N., Mandea, M., 2008. Rapidly changing flows in the Earth’s core. *Nat. Geosci.* **1**, 390–394. doi:10.1038/ngeo203.

- Pinheiro, K., Jackson, A., 2008. Can a 1D mantle electrical conductivity model generate magnetic jerk differential time delays?, *Geophys. J. Int.*, **173**(3), 781–792.
- Pinheiro, K., 2009. Mantle electrical conductivity estimates from geomagnetic jerk observation. Ph. D. Thesis, Institute of Geophysics, *Earth and Planetary Magnetism Group*. ETH Zurich. Switzerland.
- Pinheiro, K., Jackson, A., Finlay, C., 2011. Measurements and uncertainties of the occurrence time of the 1969, 1978, 1991 and 1999 geomagnetic jerks. *Geophys. Geochem. Geosyst.*, **10**. 1029/2011GC003706.
- Sabaka, T. J., Olsen, N., Langel, R., 2002. A comprehensive model of the quiet-time, near-earth magnetic field: phase 3, *Geophys. J. Int.*, **151**, 32–68.
- Sabaka, T. J., Olsen, N., Purucker, M., 2004. Extending comprehensive models of the Earth’s magnetic field with Ørsted and CHAMP data, *Geophys. J. Int.*, **159**, 521–547.
- Verbanac, G., Luhr, H., Rother, M., 2006. Evidence of the ring current effect in geomagnetic observatories annual means. *Geofizika*, **23**: 13-20.